Molecular Dynamics Simulations of the TEM-1 β-Lactamase Complexed with Cephalothin

Natalia Díaz,[†] Dimas Suárez,[†] Kenneth M. Merz, Jr.,*[,‡] and Tomás L. Sordo*[,†]

Departamento de Química Física y Analítica, Universidad de Oviedo, C/Julián Clavería 8, 33006 Oviedo, Spain, and Department of Chemistry, The Pennsylvania State University, 152 Davey Laboratory, University Park, Pennsylvania 16802-6300

Received August 5, 2004

Herein, we present theoretical results aimed at elucidating the origin of the kinetic preference for penicillins over cephalosporins characteristic of the TEM/SHV subgroup of class A β-lactamases. First, we study the conformational properties of cephalothin showing that the C2-down conformer of the dihydrothiazine ring is preferred over the C2-up one by ∼2 kcal/mol in solution (0.4−1.4 kcal/mol in the gas phase). Second, the TEM-1 β-lactamase complexed with cephalothin is investigated by carrying out a molecular dynamics simulation. The $\Delta G_{binding}$ energy is then estimated using molecular mechanics Poisson−Boltzmann surface area (MM-PBSA) and quantum chemical PBSA (QM-PBSA) computational schemes. The preferential binding of benzylpenicillin over cephalothin is reproduced by the different energetic calculations, which predict relative $\Delta\Delta G_{binding}$ energies ranging from 1.8 to 5.7 kcal/mol. The benzylpenicillin/cephalothin $\Delta\Delta G_{binding}$ energy is most likely due to the lower efficacy of cephalosporins than that of penicillins in order to simultaneously bind the "carboxylate pocket" and the "oxyanion hole" in the TEM-1 active site.

Introduction

Production of β-lactamase enzymes is the most important mechanism through which bacteria have become resistant to β-lactam antibiotics.[1,2] The β-lactamases are usually grouped into four classes, A, B, C, and D, following a molecular structure classification proposed in the early 1980s although other functional classification schemes have been proposed.[3] Classes A, C, and D are serine hydrolases whose catalytic action is characterized by a simple acyl−enzyme pathway. In the first step, an acyl−enzyme intermediate is formed between the β-lactam moiety and the conserved active site serine residue. In the second step, the acyl−enzyme intermediate is hydrolyzed by a water molecule, and finally, the active site is regenerated for the next turnover by product loss. The class B enzymes are zinc-metalloenzymes which catalyze the hydrolysis of nearly all β-lactams including the versatile broad-spectrum antibacterial carbapenem derivatives. However, the serine β-lactamases outnumber the zinc-enzymes and are considered a more immediate threat that compromises the future therapeutic usefulness of the β-lactam antibacterial agents.[4] Moreover, many extended-spectrum serine β-lactamases, which have emerged during the past decade, are able to efficiently hydrolyze third-generation cephalosporins and carbapenems.

The class A enzymes are the major culprits when it comes to destroying β-lactams, and therefore, they have been intensively studied.[5] Initially, the class A β-lactamases were thought to be better penicillinases than cephalosporinases. However, it has become apparent that class A β-lactamases are responsible for extended-spectrum antibiotic resistance in an increasing number of pathogenic bacteria including the *Serrattia*, *Enterobacter*, and *Pseudomonas* genera. Thus, it has been proposed that class A enzymes should be categorized into three subgroups according to their kinetic and structural properties as penicillinases (TEM/SHV group), cephalosporinases (PER group), and carbapenemases (NMC-A).[6] All these enzymes possess the same catalytic machinery in which the nucleophilic residue Ser70 is surrounded by several conserved residues including Lys73, Ser130, Glu166, and Lys234 and a water molecule (Wat1) bridging the Glu166 carboxylate with the Ser70 hydroxyl group (the sequence numbering of Ambler et al. is used[7]).

In an effort to increase our understanding of the structure and function of the class A β-lactamases, many X-ray structures of the apoenzymes have been solved, like TEM-1[8] and TOHO-1[9] from *Escherichia coli*, BS3 from *Bacillus licheniformis*,[10] PC1 from *Staphylococcus aureus,*[11,12] PSE-4[13] and PER-1[6] from *Pseudomonas aeruginosa*, NMC-A from *Enterobacter clocae*,[14] and so forth. In addition, high-resolution crystal structures for the acyl−enzymes have been reported. All these crystallographic structures complemented with kinetic measurements have provided structural explanations for the broadened substrate profile of the class A group of β-lactamases. For example, it has been shown that two of the most conserved structural motifs lining the active site of class A enzymes (the Ω loop and the β3 strain) are significantly altered in the PER-1 enzyme.[6] The new fold of the Ω loop and the insertion of four residues at the edge of the β-strand β3 generate a large cavity in the PER-1 enzyme that can easily accommodate the bulky substituents of extended-spectrum cephalosporins. Similarly, the TEM-like β-lactamase SHV-2,

* To whom correspondence should be addressed. For K.M.M.: phone, 814-865-3623; fax, 814-863-8403; e-mail, merz@psu.edu. For T.L.S.: phone, +34-985103475; fax, +34-985103125; e-mail, tsordo@uniovi.es.
[†] Universidad de Oviedo.
[‡] The Pennsylvania State University.

10.1021/jm0493663 CCC: $30.25
Published on Web 01/14/2005

Scheme 1

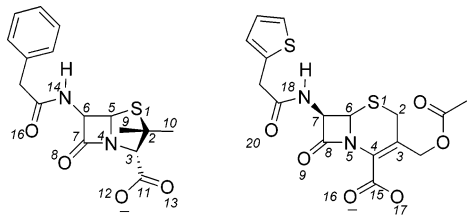

which exhibits activity against third-generation cephalosporins, accomplishes this via a Gly238Ser mutation (relative to the SHV-1 case) which displaces the β-strand β3 away from the Ω loop and results in an expansion of the β-lactam binding site.[15] However, there are other structures in which either structural changes or residue substitutions appear at regions relatively distant from the active site (e.g., the presence of an extra disulfide link in the NMC-A enzyme,[16] the Glu240Cys mutation of the TEM-1 enzyme,[17] etc.). In these cases, structural information alone has not provided a solution to the question of the origin of extended-substrate capabilities of these enzymes. Moreover, the origin of the kinetic preference for penicillins over cephalosporins in the TEM/SHV group of β-lactamases is still an open question as shown in a crystallographic study of the acyl−enzyme complexes of the *S. aureus* PC1 enzyme with benzylpenicillin and cephaloridine,[12] showing that substrate specificity is not determined at the acyl−enzyme state. This result suggests that the preference for penicillins is determined prior to the cleavage of the β-lactam ring, when the rigid fused-ring systems of the penicillins and cephalosporins form different interactions with the active site.[12]

Clearly, the specificity for one β-lactam antibiotic or another may largely depend on the structural and dynamical properties of the Michaelis complexes formed between the class A enzymes and the substrate molecules. Hence, molecular dynamics (MD) simulations constitute a valuable tool capable of determining the mobility of the active site residues, the nature and relative stability of the enzyme−substrate contacts, the location of the catalytic water molecules, the abundance of prereactive conformations, the enzyme−substrate binding energy, and so forth. In a previous work, we analyzed MD simulations of the TEM-1 β-lactamase in aqueous solution.[18] Both the free form of the enzyme and its complex with benzylpenicillin were studied showing that the conformation of the Ω loop, the interresidue contacts defining the dense H-bond network in the active site, and the enzyme−substrate interactions were very stable during the simulation time. Our simulations also gave insight into the possible pathways for proton abstraction from the Ser70 hydroxyl group.

In a continuation of our previous work,[18] we undertook studies to compare the mode of binding of penicillins and cephalosporins to class A enzymes belonging to the TEM/SHV group (penicillinases). We considered the Michaelis complexes of the TEM-1 enzyme with benzylpenicillin (BP) and cephalothin (CEF) (see Scheme 1). Both substrates are negatively charged and have neutral side chains at the C6 (BP) or C3 and C7 (CEF) positions; that is, they mainly differ in the presence of the thiazolidine ring in BP, which is replaced by the dihydrothiazine ring in CEF. Nevertheless, the overall catalytic efficiency k_{cat}/K_M of the TEM-1 enzyme is decreased by a factor of ∼50 for cephalothin hydrolysis with respect to benzylpenicillin.[17,19] In this article, we have investigated the structural and dynamical differences between benzylpenicillin and cephalothin interactions with the TEM-1 β-lactamase from *E. coli* taking advantage of the availability of MD trajectories[18] of the TEM-1/benzylpenicillin complex (TEM1−BP trajectory). First, we developed and tested a new molecular mechanics (MM) representation for cephalothin that takes into account the conformational properties of its dihydrothiazine ring and its C3 and C7 side chains. The new set of parameters for cephalothin was used to carry out an MD simulation of this antibiotic in aqueous solution. Subsequently, we computed an MD trajectory of the TEM-1/cephalothin complex (TEM1−CEF trajectory) from which the enzyme−substrate interactions were characterized and compared with those observed in the TEM1−BP complex. Relative binding free energies of the TEM1−CEF system with respect to the TEM1−BP one were obtained using the so-called molecular mechanics Poisson−Boltzmann surface area (MM-PBSA) approach that combines molecular mechanics and Poisson−Boltzmann solvation energies with molecular mechanics normal mode calculations, which account for entropic effects.[20] We also considered a variant of the MM-PBSA approach by using semiempirical quantum chemical methodologies (AM1 and PM3) to compute enthalpies and solvation energies for protein subsystems.[21,22] Comparative analyses of the enzyme−substrate contacts and binding energies in the TEM1−CEF and TEM1−BP MD trajectories allowed us to elucidate the origin of the thermodynamic effects associated with the benzylpenicillin → cephalothin substitution at the TEM-1 active site. Overall, these results give insight into the structural and dynamical changes that evolution has selected to broaden the substrate spectrum of the class A β-lactamases.

Results

Conformational Properties of Cephalothin: QM and MD Calculations. The bicyclic system of the cephalosporins can adopt two different conformations, termed C2-up and C2-down, because the C2 atom of the dihydrothiazine ring can flip between an up and a down position with respect to the plane formed by the other atoms in the ring.[23,24] The C2-up and C2-down conformations are equivalent to the axial and equatorial conformations of penicillins, respectively. For penicillins, both the crystallographic data and theoretical calculations indicate that the equatorial conformer of penicillins is biologically active. Similarly, the majority of X-ray structures of cephalosporins adopt the C2-down conformation, which suggests the biological relevance of this conformation.

To better understand the actual impact of the C2-down ↔ C2-up conformational equilibrium on the biological activity of the cephalosporins, we characterized the dihydrothiazine puckering using different theoretical approaches. Thus, we located two series of C2-down/C2-up conformers of CEF at the HF/6-31G*

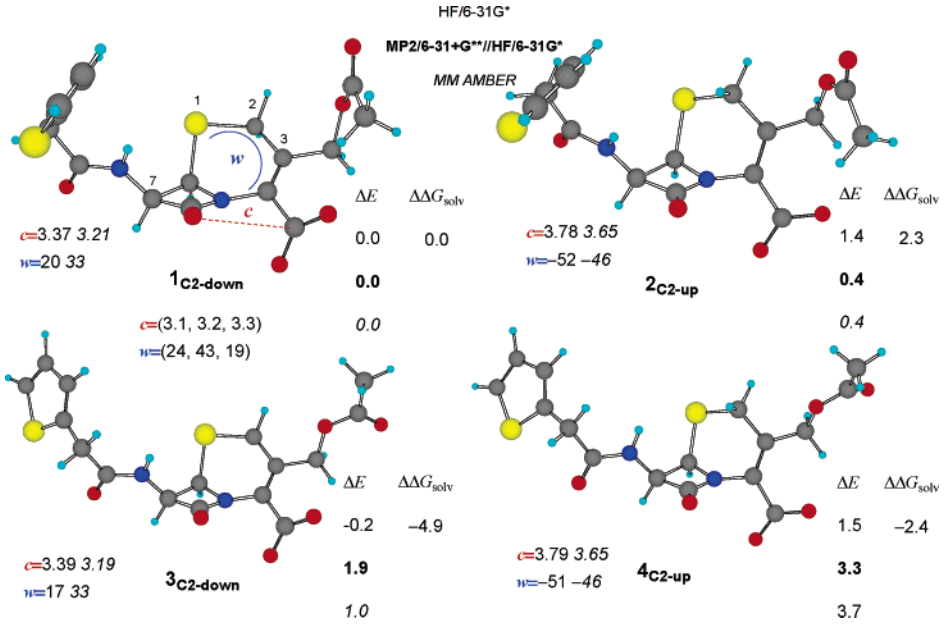

Figure 1. View of the HF/6-31G* optimized structures for the C2-down/C2-up equilibrium of cephalothin. Quantum chemical (HF/6-31G* and MP2/6-31+G**//HF/6-31G*), molecular mechanics (in italics), and SCRF solvation (ΔG_{solv}) energies (in kcal/mol) are given with respect to $\mathbf{1}_{\mathbf{C2-down}}$. The Cohen distance ($c$, in Å) and the dihydrothiazine S1−C2−C3−C4 puckering torsion angle (w, in degrees) are also indicated for the calculated minima and for the crystallographic structures (in parentheses) of cephaloridine, cephaloglycine, and cefuroxime.[65,66]

level (i.e., four structures), differing in the orientation of the two side chains at the C3 and C7 atoms (see Figure 1). The $\mathbf{1}_{\mathbf{C2-down}}$ and $\mathbf{2}_{\mathbf{C2-up}}$ structures, in which the C3 and C7 side chains are in a relatively *compact* conformation, are very close in energy (the C2-up form is 0.4 kcal/mol above the C2-down one at the MP2/6-31+G**//HF/6-31G* level). When the side chains adopt an extended form, the C2-down conformer is 1.4 kcal/mol (MP2/6-31+G**//HF/6-31G*) more stable than the C2-up conformer (see $\mathbf{3}_{\mathbf{C2-down}}$ and $\mathbf{4}_{\mathbf{C2-up}}$ in Figure 1). Hence, it turns out that the energy preference for the C2-down conformation in the gas phase is moderate and depends on the conformation of the antibiotic side chains. We used the ab initio data of the four CEF conformers to derive the corresponding AMBER parameters for CEF (RESP charges and structural data). Of course, the resulting CEF parametrization was tested by minimizing the geometry of the four conformers, the optimized MM structures being similar to the HF/6-31G* ones. For example, the root-mean-square deviation of the heavy atoms in the bicyclic nucleus between the AMBER and HF/6-31G* structures is 0.31, 0.27, 0.26, and 0.23 Å for $\mathbf{1}_{\mathbf{C2-down}}$, $\mathbf{2}_{\mathbf{C2-up}}$, $\mathbf{3}_{\mathbf{C2-down}}$, and $\mathbf{4}_{\mathbf{C2-up}}$, respectively. Similarly, the Cohen distance[25] (c) between the β-lactam O9- and C15-carboxyl atoms agrees reasonably well at the AMBER and HF/6-31G* levels of theory (see Figure 1). Figure 1 also shows that the structural parameters c and w for both C2-down conformers compare reasonably well with the values obtained from the crystallographic structures of selected cephalosporins. Energetically, the AMBER ΔE terms are in good agreement with the MP2/6-31+G**//HF/6-31G* calculations.

Single-point self-consistent-reaction-field (SCRF) calculations on the gas-phase geometries offer an estimate of solvent effects on the conformational properties of CEF: the computed solvation energies (ΔG_{solv} in kcal/mol) of the CEF conformers were −72.7 ($\mathbf{1}_{\mathbf{C2-down}}$), −70.4 ($\mathbf{2}_{\mathbf{C2-up}}$), −77.6 ($\mathbf{3}_{\mathbf{C2-down}}$), and −75.1 ($\mathbf{4}_{\mathbf{C2-up}}$). These figures suggest that the intrinsic preference of cephalosporins to adopt the C2-down conformation is reinforced by ∼2−3 kcal/mol in aqueous solution and that the extended form of the antibiotic side chains would be stabilized preferentially. To further investigate the influence of solute−solvent interactions, we carried out a 5 ns MD simulation of CEF fully solvated by a box of water molecules. The system was described classically using our AMBER-like force field for CEF and the TIP3P potential for water molecules. The large majority of the analyzed MD snapshots present the CEF molecule in its C2-down conformation (97%). In fact the C2-up structures were observed only in a short time segment (∼135 ps) at the beginning of the production run. The free energy of the C2-up conformer with respect to the C2-down one ($\Delta G_{C2-up/C2-down}$) can be directly estimated from the population of each conformer (N_{C2-up} and $N_{C2-down}$) along the MD simulations by using the following equation:

$$\Delta G_{C2-up/C2-down} = -RT \ln\left(\frac{N_{C2-up}}{N_{C2-down}}\right)$$

which gives a $\Delta G_{C2-up/C2-down}$ value of 2.0 kcal/mol in aqueous solution at 300 K. This result is in agreement with the ab initio data, confirming that solvent effects and the dynamic behavior of the puckering motions of CEF preferentially stabilize the C2-down conformation.

In contrast to the relatively rigid C2-down conformation of the dihydrothiazine ring, more conformational states for both the C3 and C7 side chains were populated as revealed by the superposition of the most important "representative clusters" of CEF in solution (see Figure 2). On the basis of their root-mean-square similarity, the representative structures account for 60% of the sampled snapshots (the thickness of the individual models is proportional to the population of the

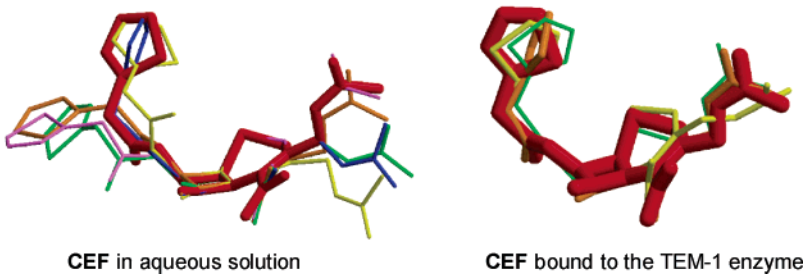

Figure 2. Superposition of the most populated representative structures derived from the clustering analyses of the free and TEM-1-complexed simulations of CEF in solution. Thickness of the models corresponds to the number of snapshots represented by each model.

Table 1. Summary of the Root-Mean-Square Deviations, Radius of Gyration, and Root-Mean-Square Fluctuations[a]

	TEM1−CEF	TEM1−BP
Root-Mean-Square Deviation		
total	1.30 ± 0.04	1.27 ± 0.04
backbone	0.81 ± 0.05	0.82 ± 0.06
subdomain α/β	1.13 ± 0.06	1.20 ± 0.07
subdomain α	1.34 ± 0.06	1.21 ± 0.05
Ω loop	0.98 ± 0.13	1.00 ± 0.09
Radius of Gyration[b]		
	17.79 ± 0.04	17.79 ± 0.04
Root-Mean-Square Fluctuation		
total	0.90 ± 0.05	0.75 ± 0.05
backbone	0.68 ± 0.05	0.55 ± 0.05
subdomain α/β	0.81 ± 0.06	0.70 ± 0.06
subdomain α	0.88 ± 0.07	0.74 ± 0.06
Ω loop	0.64 ± 0.08	0.62 ± 0.10

[a] All data are in angstroms. [b] X-ray value = 18.1.

corresponding clusters). In these structures, the two CEF side chains adopt "extended" conformations.

MD Simulation of the TEM1−CEF Complex. Table 1 collects the heavy atom root-mean-square deviations (rmsd) of the TEM1−CEF trajectory relative to the 1BLT crystal structure as well as the rms flexibility (rmsf) of the TEM-1 protein as calculated by comparing the instantaneous protein structure to the average one.[26] Both the rmsd and rmsf values were segregated into distinct structural elements (the α and α/β domains, the Ω loop, etc.). For comparative purposes, data from the TEM1−BP simulation[18] are also included. In general, we note that the structural changes in the protein were not large during the course of the TEM1−CEF simulation and that the overall protein architecture of the TEM1−BP and TEM1−CEF models was practically identical. Furthermore, the TEM1−CEF simulation gives rmsf's that hardly differ from those observed for the TEM1−BP model.

Figure 3 shows the structure of the active site region in the TEM-1 enzyme complexed with cephalothin and schematically identifies the most significant H-bond and hydrophobic contacts between the substrate and the enzyme residues. In Table 2, the enzyme−substrate H-bond contacts were characterized in terms of distances between heavy atoms and their percentage of occurrence.

The overall architecture of the active site in the presence of cephalothin is very similar to those of the free and benzylpenicillin-complexed forms of the enzyme. For example, the polar cluster around the Lys73-Glu166 pair including the Glu166-Wat1-Ser70 bridge as well as the Ser130-Lys234-Ser235 H-bonding sequence was stable in the presence of the substrate (see Figure 3a). Similarly, a water bridge connects the Arg244 guanidinium group with the carbonyl group of Val216 throughout the MD simulation. These and other contacts in the active site region have been thoroughly discussed.[18] However, it is interesting to note that the TEM1−CEF simulation shows a shorter average distance between the catalytically important Glu166 carboxylate and the nucleophilic hydroxyl group of Ser70 (Oγ@Ser70···Oϵ2@Glu166 is 3.88 ± 0.36 in TEM1−BP and 3.40 ± 0.39 in TEM1−CEF).

Figure 2 displays the most important "representative clusters" for the accessible conformations of the cephalothin molecule during the TEM1−CEF simulation, which accounts for 75% of the sampled snapshots. Thus, we see in Figure 2 that the active site of the TEM-1 enzyme does not alter the preference of the dihydrothiazine ring to adopt the C2-down conformation. It is interesting to note that, as in the case of the equatorial conformation of penicillins, the C2-down form of the CEF substrate avoids a possible steric clash with the methyl group of Ala237 and simultaneously favors the direct interaction between the substrate carboxylate and Arg244. On the other hand, the flexibility of the C3 and C7 side chains of CEF is significantly reduced upon substrate binding (see Figure 2). The C3 side chain is mainly oriented toward the solvent with its carbonyl group interacting with the Arg244 guanidinium group. The C7-acylamino side chain is partially confined by H-bond interactions with important residues (Asn132 and Ala237, see below), but flip motions of the five-membered thiophene ring occur frequently during the TEM1−CEF trajectory. In fact, the relatively large mobility of the thiophene ring prevents the CEF C7 side chain from forming a stable $\pi-\pi$ complex with the aromatic ring of Tyr105 as that observed in the TEM1−BP trajectory.[18]

As shown in Figure 3, three parts of the CEF antibiotic (i.e., the dihydrothiazine ring, the four-membered β-lactam ring, and the C7-acylamino side chain) contribute to anchor the substrate within the active site cleft. Remarkably, the negatively charged carboxylate group interacts with an array of polar and charged residues that constitute the "carboxylate pocket". Thus, the O16@CEF and O17@CEF atoms give direct H-bond interactions (X···Y distances = 2.7−3.0 Å, ∼100% abundance) with Ser130, Ser235, and Arg244, while the weakest interaction corresponds to the CEF−$COO^{-}\cdots{}^{+}{}_{3}HN$-Lys234 contact (∼3.4 Å), which is present in only 64% of the computed snapshots. On the other hand, the Ala237 NH group and the Ser70 backbone constitute the so-called "oxyanion hole". In the TEM1−

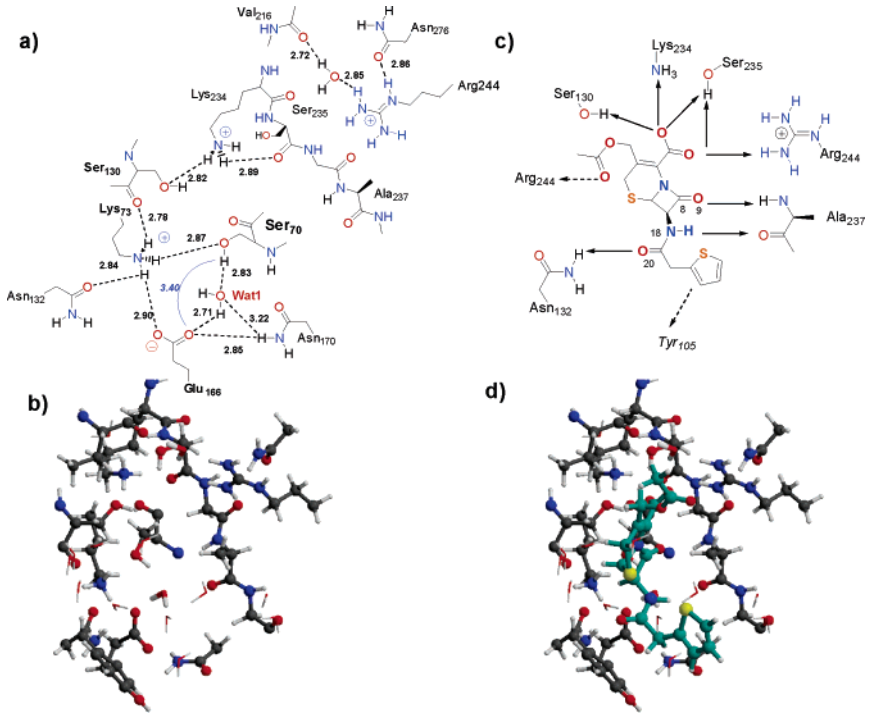

Figure 3. (a) Schematic representation of some interresidue contacts characterizing the active site of the TEM1−CEF model, (b) snapshot of the TEM1−CEF active site (CEF not shown), (c) schematic representation of the enzyme−substrate binding determinants between CEF and the TEM-1 enzyme, (d) snapshot of the TEM1−CEF active site with cephalothin shown in dark cyan.

Table 2. Summary of the Average Distances between Heavy Atoms (Å) and Percent Occurrence Data of Important Hydrogen Bonding Interactions between Cephalothin and the TEM-1 Protein[a]

	TEM1−CEF			TEM1−BP	
H-bond	X···Y	%	H-bond	X···Y	%
CEF−O16···H−Oγ-Ser130	2.68 ± 0.12	99.0	BP−O12···H−Oγ-Ser130	2.65 ± 0.11	100.0
CEF−O16···H−Oγ-Ser235	2.94 ± 0.24	98.8	BP−O12···H−Oγ-Ser235	2.82 ± 0.18	100.0
CEF−O16···H−Nζ-Lys234	3.42 ± 0.33	63.8	BP−O12···H−Nζ-Lys234	3.59 ± 0.29	53.0
CEF−O17···H−Oγ-Ser235	2.98 ±0.22	99.3	BP−O13···H−Oγ-Ser235	2.91 ± 0.19	100.0
CEF−O17···H−Nη1-Arg244	2.99 ± 0.32	97.5	BP−O13···H−Nη1-Arg244	2.79 ± 0.12	100.0
CEF−O9···H−N-Ser70	3.80 ± 0.15	36.7	BP−O8···H−N-Ser70	3.38 ± 0.27	96.4
CEF−O9···H−N-Ala237	2.84 ± 0.11	99.9	BP−O8···H−N-Ala237	2.86 ± 0.11	100.0
CEF−O9···H−O-Wat1	3.52 ± 0.25	4.1	BP−O8···H−O-Wat1	3.26 ±0.31	0.9
CEF−O20···H−Nδ-Asn132	2.98± 0.18	99.8	BP−O16···H−Nδ-Asn132	2.98 ± 0.20	95.3
CEF−O20···H−O-Wat1	3.61± 0.34	14.0	BP−O16···H−O-Wat1	3.51 ± 0.40	22.1
CEF−N18H···O=C-Ala237	3.08 ± 0.22	93.3	BP−N14···O=C-Ala237	3.10 ± 0.22	48.0

[a] Data from the TEM1−BP simulation are also included for comparison. Fluctuations correspond to standard errors of mean values.

CEF trajectory, the CEF carbonyl group interacts only with Ala237 through a stable C=O···H−N bond (see Figure 3 and Table 2), whereas the Ser70 main chain amino group hardly contributes to the orientation of the substrate carbonyl. The two specific interactions CEF−C=O···H−Nδ-Asn132 and CEF−NH···O=C-Ala237 H-bonds bind the C7 side chain of CEF.

To address the prereactive character of the Michaelis complex represented by the TEM1−CEF model, we monitored the distance between C8@CEF of the β-lactam carbonyl group (electrophile) and Oγ@Ser70 (nucleophile). The mean value for this distance was low, 3.30 ± 0.30 Å, with the closest distance being only 2.63 Å. The average Ser70@Cβ-Oγ···C8@CEF angle is 100.8 ± 7.2°, which is close to those observed for typical C−O−C bond angles. Thus, the nucleophilic group in the TEM1−CEF simulation is well positioned to attack the carbonyl carbon of the substrate.

Computation of Binding Energies. To better understand the origin of the relative penicillinase/cephalosporinase specificity of the TEM-1 β-lactamase, we carried out a thermodynamic analysis of the BP/CEF binding to the TEM-1 enzyme by applying the MM-PBSA protocol as described in Computational Details. Equivalent sampling was performed in the two 1-ns MD trajectories, TEM1−BP and TEM1−CEF, and statistical convergence of the mean values of the free energies was verified. The free energies of binding and energetic components are collected in Table 3. The MM energy terms and PB solvation energies were computed on snapshots containing the full enzymatic system (TEM-1 + β-lactam substrate), while entropic contributions were computed from selected subsystems comprising the active site region. However, by recomputing the AMBER (E_{MM}) and PBSA ($\Delta\Delta G_{solv}$ and ΔG_{surf}) energy terms on the subsystems, we were able to estimate the model dependence of the MM-PBSA free energies.

The average $\Delta G_{binding}$ energies for CEF and BP amount to −22.4 ± 7.1 and −26.8 ± 7.4 kcal/mol, respectively, when the full system is considered in the

Table 3. Average MM-PBSA Free Energy Components[a] in the TEM-1/β-Lactam Complexes[b]

		ΔE_{MM}	ΔE_{elec}	ΔE_{vdW}	$\Delta\Delta G_{solv}^{PB}$	ΔG_{surf}	$-T\Delta S_{binding}$[c]	$\Delta G_{binding}$[c]
TEM1−BP	full system	−90.9 ± 7.5	−52.5 ± 7.1	−35.4 ± 2.9	43.2 ± 4.8	−3.3 ± 0.1		−26.8 ± 7.4[d]
	subsystem	−149.1 ± 7.0	−119.7 ± 5.1	−29.5 ± 2.8	107.5 ± 4.5	−2.9 ± 0.1	22.9 ± 4.3	−20.2 ± 7.0
TEM1−CEF	full system	−79.2 ± 8.8	−40.4 ± 8.9	−38.7 ± 2.7	37.4 ± 7.4	−3.6 ± 0.2		−22.4 ± 7.1[d]
		(*11.7*)	(*12.1*)	(*−3.3*)	(*−5.8*)	(*−0.3*)		(*4.4*)
	subsystem	−138.3 ± 8.7	−107.6 ± 8.8	−30.6 ± 2.9	100.2 ± 8.2	−3.0 ± 0.1	21.2 ± 4.6	−18.1 ± 7.0
		(*11.0*)	(*12.1*)	(*−1.1*)	(*−7.3*)	(*−0.1*)	(*−1.7*)	(*2.1*)

[a] In kilocalories per mole. [b] Relative differences of the TEM1−CEF mean values with respect to the TEM1−BP ones are in parentheses. Fluctuations correspond to standard errors of mean values. [c] The standard state is to be taken as 1 M. [d] Using the entropy corrections from normal mode calculations on subsystems.

Table 4. Average AM1- and PM3-Based Free Energy Components[a] in the TEM-1/β-Lactam Complexes[b]

		$\Delta H_{binding}$	$\Delta H_{binding}$ including LJ/R^6	$\Delta\Delta G_{solv}$	$\Delta G_{binding}$[c]	$\Delta G_{binding}$[c] including LJ/R^6
TEM1−BP	AM1	−79.6 ± 6.1	−154.0 ± 8.3	100.3 ± 4.3	43.2 ± 6.0	−31.2 ± 8.5
	PM3	−86.7 ± 5.1	−161.1 ± 6.7	106.2 ± 4.1	42.1 ± 5.8	−32.3 ± 7.9
TEM1−CEF	AM1	−78.6 ± 6.9	−148.7 ± 8.8	101.9 ± 7.6	45.0 ± 5.5	−25.6 ± 7.5
		(*1.0*)	(*5.3*)	(*1.6*)	(*1.8*)	(*5.6*)
	PM3	−82.8 ± 6.7	−152.9 ± 8.5	105.1 ± 7.7	44.0 ± 6.6	−26.6 ± 4.8
		(*3.9*)	(*8.2*)	(*−1.1*)	(*2.0*)	(*5.7*)

[a] In kilocalories per mole. [b] Both data without and with the dispersion energy correction as estimated by the AMBER Lennard-Jones term are shown. Relative differences of the TEM1−CEF mean values with respect to the TEM1−BP ones are in parentheses. Fluctuations correspond to standard errors of mean values. [c] Including the entropy corrections from MM normal mode calculations on subsystems. The standard state is to be taken as 1 M.

MM-PBSA calculations. Truncation effects decrease the absolute $\Delta G_{binding}$ energies to −18.1 ± 7.0 (CEF) and −20.2 ± 7.0 (BP) kcal/mol. Nevertheless, the mean $\Delta G_{binding}$ values obtained from both the full system and subsystem MM-PBSA calculations predict that the *relative* binding affinity of CEF is lower than that of BP by 4.4 (full system) and 2.1 (subsystem) kcal/mol. Inspection of the free energy components shows that the relative binding ability of the penicillin and the cephalosporin is governed by a balance of intraprotein and solvent effects: benzylpenicillin establishes stronger enzyme−substrate interactions, while binding of CEF is favored by a lower desolvation penalty than BP.

The thermodynamic analyses were repeated for the protein subsystems in the TEM1−BP and TEM1−CEF trajectories by applying the quantum chemical methodologies Poisson−Boltzmann surface area (QM-PBSA) computational scheme, which is based on extensive linear scaling QM SCRF calculations on structures that were partially relaxed by means of QM/MM energy minimizations. Both the AM1 and PM3 semiempirical Hamiltonians were used. The average values of some QM/MM distances between the CEF/BP substrate and important residues in the TEM-1 active site are collected in Table S5 (see Supporting Information). In general, the QM/MM TEM-1 complexes were structurally similar to those generated during the MD simulations using the MM force field representation.

The QM-PBSA results are collected in Table 4. In the absence of the Lennard-Jones energy term (see Computational Details), we found that the QM-PBSA absolute values of the $\Delta G_{binding}$ energies were largely positive (∼42 kcal/mol) for the two semiempirical methods. Nevertheless, the relative $\Delta G_{binding}$ values estimated by the QM-PBSA calculations point out that benzylpenicillin is a better TEM-1 ligand than cephalothin by 1.8 (AM1) and 2.0 (PM3) kcal/mol in agreement with the prediction made by the standard MM-PBSA approach. It may be noteworthy that the AM1 and PM3 methods differ in the relative importance of enzyme−substrate ($\Delta H_{binding}$) and desolvation ($\Delta\Delta G_{solv}$) effects that determine the relative penicillin/cephalosporin affinity of TEM-1. While the lower desolvation penalty in the TEM1−CEF system cannot be compensated by the weaker enzyme−substrate interactions according to the PM3-PBSA calculations, both the enzyme−substrate forces and the desolvation penalty contribute to the reduced cephalosporin binding to the TEM-1 enzyme according to the AM1-based energies (see Table 4).

When the attractive Lennard-Jones energy term is included (account for the dispersion interactions not included in uncorrelated QM methods), the QM-PBSA $\Delta G_{binding}$ energies become clearly negative and have values close to the MM-PBSA ones (−25, −31 kcal/mol; see Table 4), showing the importance of the dispersion energy to the total $\Delta G_{binding}$. The relative $\Delta\Delta G_{binding}$ energies were also altered by the inclusion of the LJ/R^6 term, the binding energy of the BP substrate being favored by 5.6 kcal/mol over CEF.

Discussion

Comparison between Theoretical and Experimental Binding Energies. The significance of k_{cat}/K_M and K_M in the acyl−enzyme mechanism characteristic of the class A β-lactamases has been examined by Christensen et al. in their study of β-lactamase as fully efficient enzymes.[27] These authors have found that the similarity of all the first-order rate constants that characterize the general acyl−enzyme kinetic mechanism makes K_M approximately equal to the true dissociation constant K_S. Kinetic parameters of the TEM-1 β-lactamase reacting with benzylpenicillin and cephalothin under comparable experimental conditions are available from two previous works. First, Raquet et al. have reported that the thiazolidine → dihydrothiazine substitution affects both the rate of catalysis and the mode of substrate binding.[19] These authors obtained the following kinetic parameters: k_{cat} = 1600 s^{-1} and K_M = 19 μM for BP; k_{cat} = 160 s^{-1} and K_M = 246 μM for CEF. The absolute binding energies derived from the K_M values amount to −6.5 and −4.9 kcal/mol for BP and CEF, respectively (using $\Delta G_{binding} = RT \ln K_S$). In a

more recent work, Cantu et al. have studied cephalosporin binding to the TEM-1 β-lactamase.[17] The corresponding kinetic parameters for BP and CEF obtained in this work ($k_{cat} = 1284 \pm 20$ s^{-1} and $K_M = 75 \pm 8$ μM for BP; $k_{cat} = 115 \pm 3$ s^{-1} and $K_M = 347 \pm 14$ μM) roughly reproduce those previously reported by Raquet et al. and lead to $\Delta G_{binding}$ values of -5.6 and -4.7 kcal/mol for BP and CEF, respectively. Hence, according to Cantu et al., BP is a better TEM-1 ligand than CEF by 0.9 kcal/mol.

When the theoretical and experimental $\Delta G_{binding}$ energies are compared, it turns out that the MM-PBSA and QM-PBSA energies overestimate the binding energy by 15 or more kcal/mol. This is not surprising given that absolute binding free energy calculations are still very demanding and provide a stringent test to the underlying methodology used to obtain energy contributions.[28] In practice, the estimation of relative $\Delta\Delta G_{binding}$ values of related systems can be carried out with much more confidence using the MM-PBSA and QM-PBSA methods (see below). Thus, the preferential binding of BP over CEF predicted by our energetic analyses, which ranges from 1.8 to 5.7 kcal/mol (see Table 4), is in reasonable agreement with the experimental estimates of 0.9−1.5 kcal/mol. Particularly, both the MM-PBSA and *pure* QM-PBSA (i.e., no LJ/R^6 energy terms included) calculations on protein subsystems give small $\Delta\Delta G_{binding}$ energies around 2.0 kcal/mol, which are close to the experimental estimates.

The observed difference in the free energies can be now interpreted in terms of the energy components and the observed TEM-1 substrate binding interactions. In this respect, we note that the larger energy differences between BP and CEF arise either in the molecular mechanical ΔE_{elec} terms or in the semiempirical $\Delta H_{binding}$ energies. This indicates that the penicillinase ability of TEM-1 is a consequence of better electrostatic and hydrogen-bond interactions when BP binds to the active site.

Consistency of the MM-PBSA and QM-PBSA Calculations. In recent years, the combination of MD simulations with a subsequent analysis of energetic and entropic components has been applied to compute absolute binding energies and relative binding affinities between diverse ligands. These are very important problems in computational biochemistry because of their potential impact on rational drug discovery and design. In this respect, the results presented herein can be of methodological interest because they further confirm the robustness and reliability of the MM-PBSA method in order to predict small energy differences (~1−2 kcal/mol) in the binding energy of dissimilar substrate molecules. This ability of the MM-PBSA/QM-PBSA calculations to reproduce small $\Delta\Delta G_{binding}$ effects likely stems from three different factors. First, the computationally efficient particle−mesh−Ewald (PME) algorithm and the extended simulations result in realistic average structures of biomolecules in aqueous solution.[20] Second, the computation of free energies combining a well-balanced description of specific electrostatic interactions throughout the whole protein system with the robustness and reliability of the electrostatic continuum methods is based on the linearized Poisson−Boltzmann equation in order to take into account solvent effects.[20]

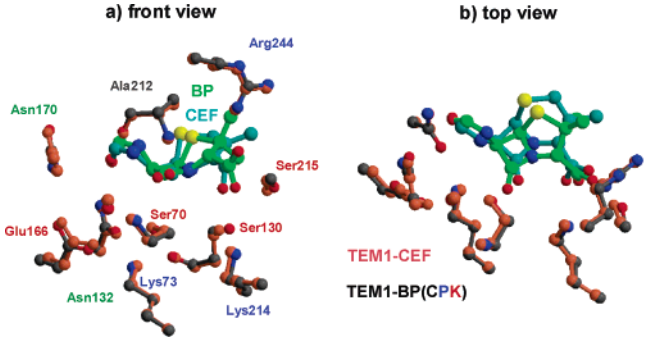

Figure 4. Superposition of the average structures derived from the TEM1−BP (in CPK colors) and TEM1−CEF (in brown) simulations showing important active site residues and the bicyclic nucleus of the CEF (in dark cyan) and BP (in green) antibacterial agents.

Third, systematic errors in the computed molecular mechanical energies/heats of formation and solvation free energies of one complex (e.g., TEM1−BP) are likely to partially cancel those of the other complex (TEM1−CEF).

Our results show that QM-based energies can be used to account for enzyme−substrate interactions using standard semiempirical Hamiltonians with only a moderate computational cost. In effect, the sampling and computational protocols, which favor cancellation of errors, appear to attenuate the well-known limitations of the semiempirical Hamiltonians (too low rotational barriers around the amide bonds, poor binding energies for hydrogen bonds, lack of dispersion interactions, etc.)[29,30] so that the *pure* QM-PBSA method can predict $\Delta\Delta G_{binding}$ energies. It is also interesting to note how the QM calculations, which incorporate charge-transfer and polarization effects, provide a *softer* description of the energy changes involved in the binding process than the MM-PBSA calculations. Additionally, the QM-PBSA approach provides a complete description of the structure and electrostatics of many classes of ligands and protein active sites, including metalloenzymes or reactive intermediates which are difficult to accurately model using molecular mechanics. Overall, the present results and former results on the development of a QM-based scoring function[22] indicate that the use of QM methodologies will allow us to go beyond the limitations of molecular mechanical force fields when evaluating protein−ligand interactions.

Comparison between the BP and CEF Binding Determinants. Figure 4 displays the superposition of the β-lactam antibacterial agents and several active site residues obtained from the average TEM1−BP and TEM1−CEF MD structures. Interestingly, the average positioning of the important residue side chains (Ser70, Lys73, Ser130, Lys234, etc.) was very similar in the two MD trajectories, reflecting the stability of the hydrogen-bond network that constitutes the architecture of the TEM-1 catalytic site (the rms deviation for the selected protein residues is 0.28 Å). Only the Glu166 carboxylate and the hydroxyl groups of Ser130 and Ser235 were slightly shifted on going from TEM1−BP to TEM1−CEF. We also see in Figure 4 that the bicyclic skeleton of the CEF molecule is significantly rotated with respect to BP, and consequently, the substrate carboxylate and, particularly, the β-lactam amide groups occupy slightly different positions in the active site. Nevertheless, this

different location of BP and CEF does not affect the binding of their respective carboxylate moieties, which give comparable long-lived hydrogen bonds with the polar residues constituting the "carboxylate pocket" throughout the TEM1−BP and TEM1−CEF MD simulations (see Table 2). In contrast, the orientation of the β-lactam carbonyl group within the "oxyanion hole" is different when comparing the average TEM1−BP and TEM1−CEF structures. Moreover, the CEF substrate does not give the C═O···HN-Ser70 interaction, while BP gives a stable H-bond with the backbone amino group of Ser70 during the TEM1−BP simulation (see Table 2 and Figure 4). Therefore, it can be concluded that the lower $\Delta G_{binding}$ energy of CEF with respect to BP is likely related to the worse interaction of CEF with the TEM-1 "oxyanion hole".

A closer examination of the superimposed β-lactam structures shows that the different orientation of cephalosporin with respect to penicillin is due to their different geometrical properties. Thus, cephalosporins have the carboxylate group closer to the β-lactam amide group than penicillins as measured by their corresponding Cohen distances,[25] which have typical values of ∼4.5 (O8···C11) and ∼3.4 (O9···C15) Å for penicillins and cephalosporins, respectively. This suggests that cephalosporins are less capable than penicillins to simultaneously bind the two anchorage points in the TEM-1 active site (i.e., the "carboxylate pocket" and the "oxyanion hole" for the β-lactam carbonyl). This is indeed the case according to our simulations and energy analyses: the strength and flexibility of the "carboxylate pocket" dominate over the "oxyanion hole" in the TEM1−CEF configuration, resulting in a good interaction between the CEF carboxylate and the protein at the cost of weakening the interaction between the CEF carbonyl group and the "oxyanion hole". From these results, a clear structure−activity relationship regarding the penicillin/cephalosporin affinity exhibited by the TEM-1 β-lactamase can be outlined: the poorer binding of cephalosporins with respect to penicillins to TEM-1 is due to unbalanced interactions of the "carboxylate pocket"/"oxyanion hole" with the β-lactam carboxylate/amide groups determined by the molecular geometry of the cephalosporins.

Penicillinase versus Cephalosporinase Activity of the Class A β-Lactamases. In their X-ray structural study of acyl−enzyme complexes of mutant forms of the *S. aureus* β-lactamase with benzylpenicillin and cephaloridine, Chen and Herzberg concluded that the acyl−enzyme structures do not account for the more rapid hydrolysis of benzylpenicillin.[12] Consequently, these authors suggested that the relative penicillinase/cephalosporinase activity of the class A β-lactamases must be determined prior to acyl−enzyme formation and that, apparently, the structural framework of the *S. aureus* enzyme is better suited to accommodate both the reactive amide group of penicillins and the β-lactam carboxylate group interacting with the "oxyanion hole" and the Lys234 ammonium group, respectively.

The theoretical results discussed above give support to the hypothesis proposed by Chen and Herzberg and shed further light on the subtle molecular details determining the preferential penicillinase activity of the class A β-lactamases. Thus, comparisons of the computed $\Delta G_{binding}$ energies of BP and CEF bound to the TEM-1 active site as well as the different "oxyanion hole"−substrate interactions emphasize the nearly perfect match between the penicillin skeleton and the TEM-1 active site crevice, which results in optimum enzyme−substrate interactions and in a carbonyl group well poised for nucleophilic attack. For cephalosporins such as cephalothin, we found that the more compact arrangement of the β-lactam amide and carboxylate groups changes the orientation of the β-lactam group within the oxyanion hole and decreases $\Delta G_{binding}$. This theoretical observation relevant to the Michaelis complexes rationalizes the experimental data on the differential binding of benzylpenicillin and cephalothin to TEM-1. However, it has also direct mechanistic implications because during nucleophilic attack of the Ser70 hydroxyl on the β-lactam carbonyl C atom the stabilization of the developing negative charge at the carbonyl O atom of the β-lactam by the backbone amide groups of Ala237 and Ser70 could be lower in the case of cephalosporins, which weakly interact with the NH group of Ser70, relative to the penicillins. This could explain the experimentally observed decrease in k_{cat} by a factor of ∼10 when comparing BP and CEF.

Table 5. Summary of Some Significant Interatomic Distances (Å) between "Carboxylate Pocket" Groups and the Backbone N Atom at the 237 Position in the Active Site of Various Class A β-Lactamases As Observed in the Corresponding X-ray Structures[a]

distance	TEM-1 (1BLT)	BS3 (1I2S)	TOHO-1 (1IYS)	NMC-A (1BUE)	TEM-64 (1JWZ)
Nζ@Lys234···N@237	7.30	7.06	6.82	6.64	6.96
Oγ@Ser130···N@237	6.64	6.81	6.56	6.51	6.47
Nη1@Arg244···N@237	4.03	4.24		4.46[c]	4.22
Oγ@Ser235···N@237	6.31	6.24[b]	6.12	5.64[c]	6.03

[a] PDB ID codes are shown in parentheses. [b] Ala237 is replaced by Thr in the BS3 enzyme. [c] In the NMC-A enzymes, Ser235 is replaced by Thr, while Arg220 is placed at the "carboxylate pocket" instead of Arg244.

Finally, we comment on the small structural changes and/or point residue mutations that presumably perturb the substrate specificity of class A β-lactamases in a subtle way by modifying the "carboxylate pocket" and the "oxyanion hole" binding sites. Particularly, we analyzed some selected interatomic distances in a series of X-ray structures of class A carbapenemases in order to measure the relative location of the "carboxylate pocket" with respect to the backbone N atom at position 237. In doing so we found that the "carboxylate pocket" is similarly rearranged in enzymes such as BS3,[10] TOHO-1,[9] NMC-A,[14] and the TEM-64 mutant.[31] Thus, Table 5 indicates that the guanidinium group of Arg244 (Arg220 in NMC-A) is consistently moved away ∼0.2−0.5 Å from the backbone amide group of residue 237, while the Lys234 ammonium group is 0.3−0.7 Å closer relative to the equivalent Arg244 and Lys234 residues in the TEM-1 enzyme (in TOHO-1 the guanidinum group is deleted by the Arg244Thr mutation). The spatial rearrangement experienced by the "carboxylate pocket" seems to be due to the accumulation of several changes: point mutations at the 235−237 positions, the presence of a disulfide bridge connecting the cysteine residues at positions 69 and 238, and so forth. Hence, the spatial rearrangement of the "carboxylate pockets", which implies the projection of the Lys234 ammonium group toward the "oxyanion hole" and the separation of

Arg244/Arg240, would be a prerequisite for a good binding of the carboxylate group of penems/carbapenems/cephalosporins while simultaneously preserving the optimal strength and orientation of the interaction between the β-lactam carbonyl and the backbone amino groups of the "oxyanion hole".

Computational Details

Quantum Mechanical Calculations. Initial coordinates for cephalothin were built by using the crystallographic structure of cephaloridine as a template. Subsequently, HF/6-31G* optimizations were carried out in the gas phase followed by single-point MP2/6-31+G** energy calculations using the Gaussian 98 suite of programs.[32] To take into account condensed-phase effects,[33] we carried out single-point MP2/6-31+G** Poisson−Boltzmann self-consistent-reaction-field (SCRF) calculations using the *local* MP2 and SCRF methods implemented in the Jaguar program.[34,35]

Molecular Mechanical Parametrization of Cephalothin. Four different conformers of CEF differing in the puckering of the dihydrothiazine ring and/or the conformation of the side chains at C3 and C7 were considered in the computation of the atomic point charges using the RESP methodology.[36] Most of the bond, angle, and dihedral parameters of CEF were available from the AMBER force field. However, some structural data required to represent the equilibrium geometry of the bicyclic skeleton of CEF were extracted from the HF/6-31G* optimized structures. The van der Waals (vdW) parameters were taken from the closest existing AMBER atom types using electronic similarity as a guide.

To further test our CEF parametrization, we computed a 5.0 ns MD trajectory of CEF fully solvated in a periodic box of 3885 TIP3P waters using the SANDER program of the AMBER 5.0 package.[37] The time step was chosen to be 1.5 fs, and the SHAKE algorithm[38] was used to constrain all bonds involving hydrogen atoms. Periodic boundary conditions were applied, and the pressure (1 atm) was controlled by Berendsen's method. To include the contributions of long-range interactions, the particle−mesh−Ewald (PME) method[39] was used with a grid size of 54 × 48 × 48 (grid spacing <1 Å) combined with a fourth-order B-spline interpolation to compute the potential and forces in between grid points. A cutoff of 10 Å was used to compute the vdW forces.

Sampled conformations from the MD trajectory were clustered using the NMRCLUST program.[40] This program uses the method of average linkage to define how clusters are constructed, followed by application of a penalty function which simultaneously minimizes (1) the number of clusters and (2) the spread across each cluster. A minimum distance of 1.5 Å was used to select representative structures from each cluster.

MD Simulation of the TEM1−CEF Complex. The determination of an initial TEM1−CEF complex was necessary to obtain a starting configuration for the MD studies. We employed the algorithm developed for AutoDock[41,42] which uses a Monte Carlo simulated annealing technique to explore the configuration space of the enzyme−ligand complex in conjunction with a rapid energy evaluation using grid-based molecular interaction potentials (built from van der Waals and electrostatic contributions). The CEF substrate was docked in the static binding site of the TEM-1 β-lactamase. During the docking process, the internal bonds of the CEF side chains were allowed to rotate. The coordinates of the protein atoms were taken from the TEM-1 1.85 Å crystal structure of Jelsch et al. (PDB ID 1BTL).[43]

The most stable enzyme−substrate complex predicted by AUTODOCK showed enzyme−substrate contacts that were favorable for binding and catalysis (e.g., the β-lactam carboxylate and carbonyl groups pointed toward Lys234 and the Ala237 amino group, respectively). This enzyme−substrate complex and the crystallographic water molecules were surrounded by a periodic box of TIP3P water molecules,[44] which extended 10 Å from the protein and substrate atoms. Six Na^+ counterions were placed by the LEaP program in order to neutralize the simulation box, which was then minimized using the parm96 version of the AMBER force field (2500 steps for the water molecules followed by 2500 steps for the entire system).[45]

MD simulations were carried out using the SANDER module of the AMBER 5.0 suite of programs.[37] The time step was 1.5 fs, and the SHAKE algorithm[38] was used to constrain all bonds involving hydrogen atoms. A nonbonded cutoff of 10 Å was used, and the nonbonded pair list was updated every 25 time steps.[46] Periodic boundary conditions were applied to simulate a continuous system. The pressure (1 atm) and the temperature (300 K) of the system were controlled during the MD simulation by Berendsen's method.[47] To include the contributions of long-range interactions, the particle−mesh−Ewald (PME) method[39] was used with a grid size of 64 × 64 × 64 (grid spacing of ~1 Å) combined with a fourth-order B-spline interpolation to compute the potential and forces in between grid points. The estimated root-mean-square deviations of the PME force errors[48] during the simulation were lower than 10^{-4}.

For the TEM1−CEF model, an equilibration period of 200 ps resulted in a stable trajectory as evidenced by the convergence of the dimensions of the simulation box and the evolution of the total energy of the system. Subsequently, a 1 ns trajectory was computed and coordinates were saved for analysis every 50 time steps. All of the MD results were analyzed using the CARNAL module of AMBER 5.0 and some other specific trajectory analysis software developed locally. The root-mean-square (rms) coordinate deviations between two structures **I** and **J** (σ_{IJ}) and the radius of gyration (R_{gyr}) of the protein complexes were computed according to the following formulas:[26]

$$\sigma_{IJ} = \sqrt{\frac{\sum_{i=1}^{N} w_i (r_i^{I} - r_i^{J})^2}{\sum_{i=1}^{N} w_i}} \qquad R_{gyr} = \sqrt{\frac{\sum_{i=1}^{N} w_i (r_i^{I} - R_C)^2}{\sum_{i=1}^{N} w_i}} \quad (1)$$

where N is the total number of atoms, w_i is the atomic mass of the i-atom, and R_C is the center of mass of the protein−substrate complex.

MM-PBSA Energetic Analyses. The molecular mechanics Poisson−Boltzmann surface area (MM-PBSA) approach in principle can perform several types of $\Delta G_{binding}$ calculations (enzyme−substrate, protein−protein, DNA−protein).[20,28,49] Basically, MM-PBSA calculations predict mean values of interaction free energies as estimated over a series of representative (~50−100) snapshots extracted from classical MD simulations. The snapshots are postprocessed through the removal of all solvent and counterions. Then, one calculates the average free energy of the set of structures according to the following equation:

$$\bar{G} \approx \bar{E}_{MM} + 3RT + \bar{G}_{PBSA} - T\bar{S}_{MM} \quad (2)$$

where $\bar{G}$ is the calculated average free energy, and $\bar{E}_{MM}$ is the average molecular mechanics energy,

$$\bar{E}_{MM} = \bar{E}_{bond} + \bar{E}_{angle} + \bar{E}_{tors} + \bar{E}_{vdW} + \bar{E}_{elec} \quad (3)$$

where these correspond to the bond, angle, torsion, van der Waals, and electrostatic terms in the molecular mechanics force field. The term $3RT$ in eq 2 corresponds to the enthalpy of the six translation and rotational degrees of freedom in the classical limit. $\bar{G}_{PBSA}$ is the solvation free energy obtained from Poisson−Boltzmann electrostatic calculations augmented with an estimate of the nonpolar free energy via molecular area, and TS_{MM} is the solute entropy which can be estimated by molecular mechanics normal mode calculations and standard statistical mechanical formulas.[20] Subsequently, one can es-

timate the ΔG for ligand association to proteins using the following equation:

$$\Delta G = \bar{G}_{\text{complex}} - \bar{G}_{\text{protein}} - \bar{G}_{\text{ligand}} \quad (4)$$

where the three G terms are usually evaluated using the snapshots from a *single* MD trajectory of the complex (the *one* trajectory approximation). Here, the binding free energies are computed for a standard state of 1 M. As a consequence, the translational entropy for each component (*complex, protein, ligand)* is 6.4 cal mol^{-1} K^{-1} smaller than the entropy value obtained for the standard state of an ideal gas owing to the change in concentration from 0.045 M (ideal gas) to 1 M (solution).[28]

In this work a set of 50 representative structures extracted every 20 ps along the TEM1−CEF MD trajectory and a second set of equivalent snapshots from the TEM1−BP simulation[18] were postprocessed to calculate the binding free energies of cephalothin and benzylpenicillin, respectively, using the MM-PBSA approach. For each system, two series of MM-PBSA calculations were performed: the first array of calculations included the entire enzyme−substrate system, while the second one deals with a protein *subsystem*. This subsystem was formed by all residues within a distance of 9 Å to Oγ@Ser70 including most of the residues in the Ω loop (residues: 68−76, 103−107, 125−135, 161−174, 234−248). Terminal *N*-methylamine or acetyl groups were placed at the C and N backbone atoms of those residues cleaved from the protein main chain by the truncation process. In addition, the BP/CEF substrate and the Wat1 molecule were also extracted.

In the MM-PBSA calculations, the AMBER force field was used to compute (no cutoff) the E_{MM} terms defined in eq 3. The electrostatic contribution to the solvation free energy ($\Delta G°_{\text{solv}}$) of the TEM1−BP and TEM1−CEF states were determined with the Poisson−Boltzmann approach which represents the protein−substrate complexes as a low dielectric continuum (a value of $\epsilon_{\text{int}} = 1$ was used in the calculations) with embedded charges and the solvent as a high dielectric continuum ($\epsilon_{\text{out}} = 80$) with no salt. Atomic charges were taken from the AMBER MM representation of the TEM1−BP and TEM1−CEF states. Because of the small size of the hydrogen atoms in the AMBER force field, the van der Waals surface used in the PB calculations was constructed using DREIDING van der Waals radii for C, H, N, O, and S atoms.[50] The dielectric boundary is the contact surface between the radii of the solute and the radius (1.4 Å) of a water probe molecule. The DELPHI 2.0 program was employed to solve the linearized PB equation on a cubic lattice by using an iterative finite-difference method (500 iterations were performed for each calculation).[51] The cubic lattice had a grid spacing of 0.5 Å and was scaled such that its dimensions were 80% larger than the longest dimension of the solute. The points at the boundary of the grid were set to the sum of Debye−Huckel potentials.

Solute entropic contributions were estimated only for the subsystem series (∼1100 atoms) using the nmode module of the AMBER 5.0 package. This program uses the normal modes and standard statistical thermodynamic formulas to estimate entropic contributions. Prior to the normal mode calculations, the geometries of the TEM1−BP/TEM1−CEF subsystems described by their AMBER representations were minimized until the root-mean-square deviation of the elements in the gradient vector was less than 10^{-5} kcal/(mol Å). The ROAR 2.0 program[52] was used to carry out the geometry optimizations driven by a limited memory BFGS minimizer.[53] All minimizations and normal mode calculations were carried out with a distance-dependent dielectric constant ($\epsilon = 4r$) to mimic solvent screening with no cutoff for the nonbonded interactions. As noted in previous work,[54] this normal mode analysis only approximately estimates solute entropy.

Semiempirical QM-PBSA Calculations. Semiempirical QM calculations can also be used to estimate the relative energies of the different protein configurations. This can be done by using linear scaling QM methodologies.[55] Thus, the free energy of the enzyme−substrate systems can be estimated according to the following equation:

$$\bar{G} \approx \bar{H}_{\text{QM}} + \Delta\bar{G}_{\text{solv}} - T\bar{S}_{\text{MM}} \quad (5)$$

where $\bar{G}$ is the calculated average free energy, $\bar{H}_{\text{QM}}$ is the average QM heat of formation of the solute which accounts for intraprotein and enzyme−substrate effects, $\Delta\bar{G}_{\text{solv}}$ is the average solvation energy, which can be calculated using the QM Hamiltonian coupled to a continuum model, and $T\bar{S}_{\text{MM}}$ is the solute entropy which can be estimated by molecular mechanics normal mode calculations. To complement the semiempirical QM energy, dispersive nonpolar interactions can be accounted for[22] by adding the attractive part of the Lennard-Jones potential using the AMBER force field to eq 4,

$$\bar{G} \approx \bar{H}_{\text{QM}} + \frac{\text{LJ}}{R^6} + \Delta\bar{G}_{\text{solv}} - T\bar{S}_{\text{MM}} \quad (6)$$

Both eqs 5 and 6 were considered in the QM-PBSA energy calculations.

Prior to the QM-PBSA calculations, the selected set of TEM1−BP and TEM1−CEF snapshots were subject to QM/MM energy minimization in which the BP/CEF substrates, the Wat1 molecule, and the side chains of Ser70, Ser130, Glu166, Lys73, Lys234, and Arg244 (QM region) were relaxed, while the rest of the protein and a solvent cap of 1500 water molecules centered on the Oγ@Ser70 atom (MM region) were held fixed. In these calculations, both the AM1[56] and PM3[57] Hamiltonians were used to describe the QM region, and the AMBER force field was used for the rest of the system. Hydrogen link atoms were placed at the corresponding Cβ atoms to cap exposed valence sites due to bonds which cross the QM−MM boundary. The ROAR 2.0 program[52] was used to carry out the QM/MM minimizations.

From the QM/MM relaxed structures, we built the enzyme−substrate subsystems described above. Then single-point AM1 and PM3 calculations were performed on these subsystems using the divide and conquer (D&C) approach.[58−60] Incorporation of solvent effects within a QM methodology was accomplished by merging the D&C algorithm with the PB equation.[61] In these QM-PB calculations, the solute was represented by charge model 2 (CM2) atomic charges.[62] The set of DREIDING atomic radii was used again in the QM-PB calculations. An additional "nonpolar" contribution due to the creation of a solute cavity in the continuum was accounted for by a term proportional to the solvent accessible surface area of the solute as in the MM-PBSA approach. The DivCon99 program[63] was employed to perform the D&C semiempirical calculations using the dual buffer layer scheme (inner buffer layer of 4.0 Å and an outer buffer layer of 2.0 Å) with one protein residue per core. This D&C *subsetting* with a total buffer region of 6.0 Å gives accurate relative energies.[64] A cutoff of 9.0 Å was used for the off-diagonal elements of the Fock, one-electron, and density matrices. Solute entropic contributions were taken from the AMBER normal mode calculations on the subsystems taken from the trajectories.

Acknowledgment. The authors are grateful to the CICyT (Spain) for a generous allocation of computer time at the CESCA and the CIEMAT. Financial support by MCyT (Spain) via Grant No. SAF2001-3526 is also acknowledged. K.M.M thanks the NIH for support of this project via Grant No. GM44974.

Supporting Information Available: Tables showing selected interatomic distances in the TEM-1 active site during the TEM1−CEF simulation, the rms flexibilities of important residues, the first peak position of $g(r)$ and its integrated value, selected interatomic distances in the QM/MM minimized structures, and so forth and a ZIP file containing the cephalothin parameters in a format suitable for the LEaP program.

This material is available free of charge via the Internet at http://pubs.acs.org.

References

(1) Walsh, C. Molecular mechanisms that confer antibacterial drug resistance. *Nature* **2000**, *406*, 775−781.
(2) Wright, G. D. Resisting resistance: New chemical strategies for battling superbugs. *Chem. Biol.* **2000**, *7*, 127−132.
(3) Bush, K. A functional classification scheme for β-lactamases and its correlation with molecular structure. *Antimicrob. Agents Chemother.* **1995**, *39*, 1211−1233.
(4) Maiti, S. N.; Philips, O. A.; Micetich, R. G.; Livermore, D. M. β-Lactamase inhibitors: Agents to overcome bacterial resistance. *Curr. Med. Chem.* **1998**, *5*, 441−456.
(5) Matagne, A.; Lamotte-Brasseur, J.; Frère, J. M. Catalytic properties of class A β-lactamases: Efficiency and diversity. *Biochem. J.* **1998**, *330*, 581−598.
(6) Tranier, S.; Bouthors, A.-M.; Maveyraud, L.; Guillet, V.; Sougakoff, W.; Samama, J.-P. The high resolution crystal structure for class A β-lactamase PER-1 reveals the bases for its increase in breadth of activity. *J. Biol. Chem.* **2000**, *275*, 28075−28082.
(7) Ambler, R. P.; Coulson, A. F.; Frére, J. M.; Ghuysen, J. M.; Jaurin, B.; Joris, B.; Levesque, R.; Tiraby, G.; Waley, S. G. A standard numbering scheme for the class A β-lactamases. *Biochem. J.* **1991**, *276*, 269−272.
(8) Fonzé, E.; Charlier, P.; To'th, Y.; Vermiere, M.; Raquet, X.; Dubus, A.; Frère, J.-M. TEM1 β-lactamase structure solved by molecular replacament and refined structure of the S235A mutant. *Acta Crystallogr., Sect. D* **1995**, *51*, 682−694.
(9) Shimamura, T.; Ibuka, A.; Fushinobu, S.; Wakagi, T.; Ishiguro, M.; Ishii, Y.; Matsuzawa, H. Acyl-intermediate structures of the extended-spectrum class A β-lactamase, TOHO-1, in complex with cefotaxime, cephalothin, and benzylpenicillin. *J. Biol. Chem.* **2002**, *277*, 46601−46608.
(10) Fonzé, E.; Vanhove, M.; Dive, G.; Sauvage, E.; Frère, J.-M.; Charlier, P. Crystal structure of the *Bacillus licheniformis* BS3 class A β-lactamase and of the acyl-enzyme adduct formed with cefoxitin. *Biochemistry* **2002**, *41*, 1877−1885.
(11) Herzberg, O. Refined crystal structure of β-lactamase from *Staphylococcus aureus* at 2.0 Å resolution. *J. Mol. Biol.* **1991**, *217*, 701−719.
(12) Chen, C. C. H.; Herzberg, O. Structures of the acyl-enzyme complexes of the *Staphylococcus aureus* β-lactamase mutant glu166asp:asn170gln with benzylpenicillin and cephaloridine. *Biochemistry* **2001**, *40*, 2351−2358.
(13) Lim, D.; Sanschagrin, F.; Passmore, L.; De Castro, L.; Levesque, R. C.; Strydnadka, N. C. J. Insights into the molecular basis for the carbenicillinase activity of PSE-4 β-lactamase from crystallographic and kinetic studies. *Biochemistry* **2001**, *40*, 395−402.
(14) Swarém, P.; Maveyraud, L.; Raquet, X.; Cabantous, S.; Duez, C.; Pédelacq, J.-D.; Mariotte-Boter, S.; Mourey, L.; Labia, R.; Nicolas-Chanoine, M.-H.; Nordmann, P.; Frère, J.-M.; Samama, J.-P. X-ray analysis of the NMC-A β-lactamase at 1.64 angstrom resolution, a class A carbapenemase with broad substrate specificity. *J. Biol. Chem.* **1998**, *273*, 26714−26721.
(15) Nukaga, M.; Mayama, K.; Hujer, A. M.; Bonomo, R. A.; Knox, J. R. Ultrahigh resolution structure of a class A β-lactamase: On the mechanism and specificity of the extended-spectrum SHV-2 enzyme. *J. Mol. Biol.* **2003**, *329*, 289−301.
(16) Raquet, X.; Lamotte-Brasseur, J.; Bouilleme, F.; Frere, J.-M. A disulfide bridge near the active site of carbapenem-hydrolyzing class A β-lactamases might explain their unusual substrate profile. *Proteins: Struct., Funct., Genet.* **1997**, *27*, 47−58.
(17) Cantu, C.; Huang, W.; Palzkill, T. Cephalosporin substrate specificity determinants of TEM-1 β-lactamase. *J. Biol. Chem.* **1997**, *272*, 29144−29150.
(18) Díaz, N.; Sordo, T. L.; Merz, K. M. J.; Suárez, D. Insights into the acylation mechanism of class A β-lactamases from molecular dynamics simulations of the TEM-1 enzyme complexed with benzylpenicillin. *J. Am. Chem. Soc.* **2003**, *125*, 672−684.
(19) Raquet, X.; Lamotte-Brasseur, J.; Fonzé, E.; Goussard, S.; Couvalin, P.; Frére, J.-M. TEM β-lactamase mutants hydrolising third-generation cephalosporins. *J. Mol. Biol.* **1994**, *244*, 625−639.
(20) Kollman, P. A.; Massova, I.; Reyes, C.; Kuhn, B.; Huo, S.; Chong, L.; Lee, M.; Lee, T.; Duan, Y.; Wang, W.; Donini, O.; Cieplak, P.; Srinivasan, J.; Case, D. A.; Cheatham, T. E. Calculating structures and free energies of complex molecules: Combining molecular mechanics and continuum models. *Acc. Chem. Res.* **2000**, *33*, 889−897.
(21) Suárez, D.; Brothers, E. N.; Merz, K. M. J. Quantum chemical calculations and molecular dynamics simulations of the dinuclear zinc-β-lactamase from *Bacteroides fragilis*. *Biochemistry* **2002**, *41*, 6615−6630.
(22) Raha, K.; Merz, K. M., Jr. A quantum mechanics-based scoring function: Study of zinc ion-mediated ligand binding. *J. Am. Chem. Soc.* **2004**, *126*, 1020−1021.
(23) Boyd, D. B. *Chemistry and Biology of β-Lactam Antibiotics*; Academic Press: New York, 1982; pp 437−545.
(24) Frau, J.; Donoso, J.; Muñoz, F.; García Blanco, F. Theoretical calculations of β-lactam antibiotics part 2. AM1, MNDO, and MINDO/3 calculations of some cephalosporins. *J. Mol. Struct. (THEOCHEM)* **1991**, *251*, 205−218.
(25) Cohen, N. C. β-lactam antibiotics: Geometrical requirements for antibacterial activities. *J. Med. Chem.* **1983**, *26*, 259−264.
(26) Field, M. J. *A practical introduction to the simulation of molecular systems*; Cambridge University Press: Cambridge, U.K., 1999; pp 25−42.
(27) Christensen, H.; Martin, M. T.; Waley, S. G. β-lactamases as fully efficient enzymes. Determination of all the rate constants in the acylenzyme mechanism. *Biochem. J.* **1990**, *266*, 853−861.
(28) Gohlke, H.; Case, D. A. Converging free energy estimates: MM-PB(GB)SA studies on the protein−protein complex ras−raf. *J. Comput. Chem.* **2003**, *25*, 238−250.
(29) Möhle, K.; Hofmann, H.-J.; Thiel, W. Description of peptide and protein secondary structures employing semiempirical methods. *J. Comput. Chem.* **2001**, *22*, 509−520.
(30) Winget, P. C. S.; Horn, A. H. M.; Martin, B.; Clark, T. Towards a "next generation" neglect of diatomic differential overlap based semiempirical molecular orbital technique. *Theor. Chem. Acc.* **2003**, *10*, 254−266.
(31) Wang, X.; Minasov, G.; Blázquez, J.; Caselli, E.; Prati, F.; Shoichet, B. K. Recognition and resistance in TEM β-lactamase. *Biochemistry* **2003**, *42*, 8434−8444.
(32) Frisch, M. J.; Trucks, G. W.; Schlegel, H. B.; Scuseria, G. E.; Robb, M. A.; Cheeseman, J. R.; Zakrzewski, V. G.; Montgomery, J. A., Jr.; Stratmann, R. E.; Burant, J. C.; Dapprich, S.; Millam, J. M.; Daniels, A. D.; Kudin, K. N.; Strain, M. C.; Farkas, O.; Tomasi, J.; Barone, V.; Cossi, M.; Cammi, R.; Mennucci, B.; Pomelli, C.; Adamo, C.; Clifford, S.; Ochterski, J.; Petersson, G. A.; Ayala, P. Y.; Cui, Q.; Morokuma, K.; Malick, D. K.; Rabuck, A. D.; Raghavachari, K.; Foresman, J. B.; Cioslowski, J.; Ortiz, J. V.; Stefanov, B. B.; Liu, G.; Liashenko, A.; Piskorz, P.; Komaromi, I.; Gomperts, R.; Martin, R. L.; Fox, D. J.; Keith, T.; Al-Laham, M. A.; Peng, C. Y.; Nanayakkara, A.; Gonzalez, C.; Challacombe, M.; Gill, P. M. W.; Johnson, B. G.; Chen, W.; Wong, M. W.; Andres, J. L.; Head-Gordon, M.; Replogle, E. S.; Pople, J. A. *Gaussian 98*, revision A.6; Gaussian, Inc.: Pittsburgh, PA, 1998.
(33) Tomasi, J.; Persico, M. Molecular interactions in solution: An overview of methods based on continuous distributions of the solvent. *Chem. Rev.* **1994**, *94*, 2027−2094.
(34) Tannor, D. J.; Marten, B.; Murphy, R.; Friesner, R. A.; Sitkoff, D.; Nicholls, A.; Ringnalda, M.; Goddard, I. W. A.; Honig, B. Accurate first principles calculation of molecular charge distributions and solvation energies from ab initio quantum mechanics and continuum dielectric theory. *J. Am. Chem. Soc.* **1994**, *116*, 11875−11882.
(35) *Jaguar*, version 3.5; Schrödinger, Inc.: Portland, OR, 1998.
(36) Bayly, C. A.; Cieplak, P.; Cornell, W. D.; Kollman, P. A. A well behaved elestrostatic potential based method using charge restraints for deriving atomic charges: The RESP model. *J. Phys. Chem.* **1993**, *97*, 10269−10280.
(37) Case, D. A.; Pearlman, D. A.; Caldwell, J. W.; Cheatham, T. E., II; Ross, W. S.; Simmerling, C. L.; Darden, T. A.; Merz, K. M., Jr.; Stanton, R. V.; Cheng, A. L.; Vincent, J. J.; Crowley, M.; Ferguson, D. M.; Radmer, R. J.; Seibel, G. L.; Singh, U. C.; Weiner, P. K.; Kollman, P. A. *Amber*, 5th ed.; University of California: San Francisco, CA, 1997.
(38) van Gunsteren, W. F.; Berendsen, H. J. C. Algorithm for macromolecular dynamics and constraint dynamics. *Mol. Phys.* **1977**, *34*, 1311−1327.
(39) Essman, V.; Perera, L.; Berkowitz, M. L.; Darden, T.; Lee, H.; Pedersen, L. G. A smooth particle-mesh-Ewald method. *J. Chem. Phys.* **1995**, *103*, 8577−8593.
(40) Kelley, L. A.; Gardner, S. P.; Sutcliffe, M. J. An automated approach for clustering an ensemble of NMR-derived protein structures into conformationally-related subfamilies. *Protein Eng.* **1996**, *9*, 1063−1065.
(41) Morris, G. M.; Goodsell, D. S.; Halliday, R. S.; Huey, R.; Hart, W. E.; Belew, R. K.; Olson, A. J. Automated docking using a Lamarckian genetic algorithm and empirical binding free energy function. *J. Comput. Chem.* **1998**, *19*, 1639−1662.
(42) Goodsell, D. S.; Olson, A. J. Automated docking of substrates to proteins by simulated annealing. *Proteins: Struct., Funct., Genet.* **1990**, *8*, 195−202.
(43) Jelsch, C.; Mourey, L.; Masson, J. M.; Samama, J. P. Crystal structure of *Escherichia coli* TEM-1 β-lactamase at 1.8 Å resolution. *Proteins: Struct., Funct., Genet.* **1993**, *16*, 364−383.
(44) Jorgensen, W. L.; Chandrasekhar, J.; Madura, J.; Impey, R. W.; Klein, M. L. Comparison of simple potential functions for the simulation of liquid water. *J. Chem. Phys.* **1983**, *79*, 926−935.

(45) Kollman, P. A.; Dixon, R.; Cornell, W.; Fox, T.; Chipot, C.; Pohorille, A. The development/application of a "minimalist" organic/biochemical molecular mechanic force field using a combination of ab initio calculations and experimental data. *Computer Simulation of Biomolecular Systems*; Kluger: Dordrecht, The Netherlands, 1997; pp 83−96.
(46) Allen, M. P.; Tildesley, D. J. *Computer simulation of liquids*; Clarendon Press: Oxford, U.K., 1987.
(47) Berendsen, H. J. C.; Potsma, J. P. M.; van Gunsteren, W. F.; DiNola, A. D.; Haak, J. R. Molecular dynamics with coupling to and external bath. *J. Chem. Phys.* **1984**, *81*, 3684−3690.
(48) Petersen, H. G. Accuracy and efficiency of the particle-mesh-ewald method. *J. Chem. Phys.* **1995**, *103*, 3668−3679.
(49) Baginski, M.; Fogolari, F.; Briggs, J. M. Electrostatic and non-electrostatic contributions to the binding free energies of anthracycline antibiotics to DNA. *J. Mol. Biol.* **1997**, *274*, 253−267.
(50) Rappé, A. K.; Casewit, C. J.; Colwell, K. S.; Goddard, W. A., III; Skiff, W. M. UFF, a full periodic table force field for molecular mechanics and molecular dynamics simulations. *J. Am. Chem. Soc.* **1992**, *114*, 10024−10035.
(51) Sharp, K. A.; Honig, B. Electrostatic interactions in macromolecules—Theory and applications. *Annu. Rev. Biophys. Biophys. Chem.* **1990**, *19*, 301−332.
(52) Cheng, A.; Stanton, R. S.; Vincent, J. J.; van der Vaart, A.; Damodaran, K. V.; Dixon, S. L.; Hartsough, D. S.; Mori, M.; Best, S. A.; Monard, G.; Garcia, M.; Van Zant, L. C.; Merz, K. M. J. *Roar 2.0*; The Pennsylvania State University: University Park, PA, 1999.
(53) Lui, D. C.; Nocedal, J. On the limited memory BFGS method for large scale optimization. *Math. Programming* **1989**, *45*, 503−528.
(54) Chong, L. T.; Duan, Y.; Wang, L.; Massova, I.; Kollman, P. A. Molecular dynamics and free energy calculations applied to affinity maturation in antibody 48g7. *Proc. Natl. Acad. Sci. U.S.A.* **1999**, *96*, 14330−14335.
(55) Goedecker, S. Linear scaling electronic structure methods. *Rev. Mod. Phys.* **1999**, *71*, 1085−1123.
(56) Dewar, M. J. S.; Zoebisch, E. G.; Healy, E. F.; Stewart, J. J. P. AM1: A new general purpose quantum mechanical molecular model. *J. Am. Chem. Soc.* **1985**, *107*, 3902−3909.
(57) Stewart, J. J. P. Optimization of parameters for semiempirical methods I. Method. *J. Comput. Chem.* **1989**, *10*, 209−220.
(58) Yang, W.; Lee, T.-S. A density-matrix form of the divide-and-conquer approach for electronic structure calculations of large molecules. *J. Chem. Phys.* **1995**, *103*, 5674−5678.
(59) Dixon, S. L.; Merz, K. M., Jr. Semiempirical molecular orbital calculations with linear system size scaling. *J. Chem. Phys.* **1996**, *104*, 6643−6649.
(60) Dixon, S. L.; Merz, K. M., Jr. Fast, accurate semiempirical molecular orbital calculations for macromolecules. *J. Chem. Phys.* **1997**, *107*, 879−893.
(61) Gogonea, V.; Merz, K. M., Jr. Fully quantum mechanical description of proteins in solution. Combining linear scaling quantum mechanical methodologies with the Poisson-Boltzmann equation. *J. Phys. Chem. A* **1999**, *103*, 5171−5178.
(62) Li, J.; Cramer, C. J.; Truhlar, D. G. New class IV charge model for extracting accurate partial charges from wave functions. *J. Phys. Chem. A* **1998**, *102*, 1820−1831.
(63) Dixon, S. L.; van der Vaart, A.; Gogonea, V.; Vincent, J. J.; Brothers, E. N.; Suárez, D.; Westerhoff, L. M.; Merz, K. M. J. *Divcon99*; The Pennsylvania State University: University Park, PA, 1999.
(64) van der Vaart, A.; Suárez, D.; Merz, K. M., Jr. Critical assessment of the performance of the semiempirical divide and conquer method for single point calculations and geometry optimizations of large chemical systems. *J. Chem. Phys.* **2000**, *113*, 10512−10523.
(65) Sweet, R. M.; Dahl, L. F. Molecular architecture of the cephalosporins. Insights into biological activity based on structural investigations. *J. Am. Chem. Soc.* **1970**, *92*, 5489−5507.
(66) Gordon, E.; Mouz, N.; Duée, E.; Dideberg, O. The crystal structure of the penicillin binding protein 2x from *Streptococcus pneumoniae* and its acylenzyme form: Implication in drug resistance. *J. Mol. Biol.* **2000**, *299*, 477−485.

JM0493663